A Study of Carbonized Lignin as an Alternative to Carbon Black

Michael R. Snowdon,[†,§] Amar K. Mohanty,[†,‡,§] and Manjusri Misra*,[†,‡,§]

[†]Department of Plant Agriculture, Crop Science Building, [‡]School of Engineering, Thornbrough Building, and [§]Bioproducts Discovery and Development Centre, University of Guelph, Guelph N1G2W1, Ontario, Canada

ABSTRACT: The production of biobased carbonaceous powder from bioethanol coproduct lignin for use as a substitute for fossil fuel-derived conductive carbon black filler is examined. The synthesis procedure used for the formation of biobased carbon black is studied in order to obtain properties similar to conventional carbon black. Characterization of the carbon material after varying carbonization temperatures and ball milling times was investigated to optimize carbon size, surface area, and thermal and electrical conductivity. The optimized carbonized ball milled lignin had a carbon content greater than 90% with the majority of the carbon atoms in the sp^2 hybridized state. The carbonized ball milled lignin exhibited a surface area 882% larger and a thermal conductivity 36% greater in comparison to the conductive carbon black tested, while the electrical conductivity was 9.5 S m^{-1} lower for the carbonized ball milled lignin. This research has demonstrated the possibility of producing biobased carbon black as a potential substitute for commercial carbon black by using lignin as a precursor material.

KEYWORDS: *Lignin, Coproduct, Carbonization, Ball milling, Thermal conductivity, Electrical conductivity, Biobased nanoparticles*

Sample		Surface Area (m² g⁻¹)
Untreated	Lignin	2
Carbonization Temperature of Lignin (°C)	600	5
	750	42
	900	654
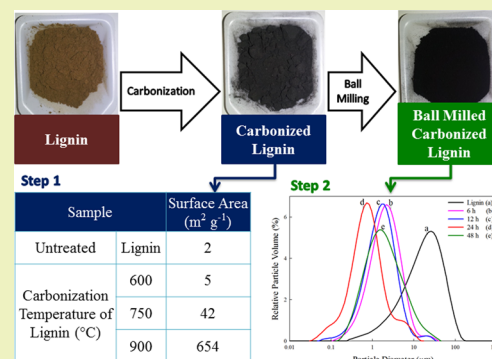
INTRODUCTION

In the past decade, nanotechnology has enabled industry and academia to develop a larger focus on nanostructured materials. Of the vast array of nanoparticles, carbon-based nanostructures remain one of the most widely studied areas in the field of nanotechnology as new uses are continually being developed.[1] These carbon nanoparticles include materials known as nanotubes, nanofibers, graphene, carbon blacks, and fullerenes.[2] In the case of carbon black, over 8 million metric tons are produced annually worldwide for a large range of applications.[3] One of the primary uses of carbon black is as filler in elastomers and plastics to enhance their overall properties.[4] Carbon black is also well known for being one of the most commonly used fillers in the production of conductive polymer composites as it tends to be a very good electrical conductor.[5,6] There are several types of carbon blacks, and they differ based on their characteristic properties ranging from surface area to particle size to conductivity. The types of carbon blacks that are predominantly used in the rubber and polymer composite sectors are furnace and thermal blacks.[7] Both furnace and thermal carbon blacks are made by incomplete combustion or thermal degradation by pyrolysis using liquid or gas hydrocarbons.[8] Concerns about global warming due to fossil fuels usage and the large reliance of carbon blacks on petroleum supplies and its increasing prices have encouraged scientists to find viable ecofriendly carbon alternatives.

Research into the use of lignin as a renewable carbon source for the production of carbon fibers and activated carbons is still ongoing.[9,10] This is partially a result of the ease in which carbon structures can be made from lignin, as the polymer has a high carbon content of approximately 60 wt %.[11] Another feature of lignin is that it is the second most abundant natural polymer in the world, and it is readily available, as large quantities are being produced as a coproduct of the pulp and paper and bioethanol industries.[12,13] By finding high value-added applications that are economically beneficial for these copious amounts of lignin, a reduction in environmental damage from unused lignin can be avoided.[14,15] Utilization of this waste lignin, which is primarily used as a fuel source in the production of in-plant electricity or discarded in landfills, will allow for a more sustainable disposal method.[16,17]

In the present study, the preparation of carbonized bioethanol coproduct lignin in the absence of any metal catalysts was studied for use as a possible carbon black alternative. The carbonization and ball milling conditions of the resulting carbonaceous material was also investigated. The carbon structures were characterized and chosen based on high surface area, small particle size, and electrical conductivity, as these are considered to be the most important properties of carbon blacks.[4]

EXPERIMENTAL SECTION

Materials. The hydrolysis lignin used in this study was pretreated Poplar hydrolysate solid residue from Mascoma, Canada, bioethanol plant with a 55% to 57% dry content that had been frozen before use. The coproduct contained approximately 62.5 wt % lignin with the remainder being nonhydrolyzed carbohydrates.[17] C-NERGY Super P

Li carbon black (CB) from Timcal, Ltd. was used for comparative purposes.

Lignin Carbonization. Prior to carbonization, the material was initially thawed in an oven at 105 °C for 24 h until dry (~50% weight reduction). The material was then ground in a planetary ball mill (Retsch PM100) with four 40 mm diameter balls at 250 rpm for 2 h with counter-rotation occurring after 1 h to reduce the size of the large particles to a powder consistency. Hydrolysis lignin was placed in a combustion boat and inserted into the center of a horizontal tube furnace (Carbolite 1200 °C G-range). The tube was sealed at both ends, and nitrogen gas was flushed through the tube to remove any oxygen in order to attain pyrolysis conditions. With a continual nitrogen gas flow through the tube, the furnace was set to a heating rate of 20 °C min^{-1} until the respective carbonization temperature was reached (600, 750, 900 °C) and remained isothermal at the given temperature for 6 h before cooling to room temperature under N_2 flow. The carbonized material was removed from the furnace upon reaching room temperature and characterized to determine the optimum carbonization temperature for the purpose of a stable conductive particle with a large surface area.

Ball Milling of Carbonized Lignin. After temperature optimization of the carbonization process was complete, the carbonized material from the chosen temperature of 900 °C was then tested in the planetary ball mill (Retsch PM100) to determine the optimum ball milling time for reduction of particle size. The various ball milling time intervals were tested using 10 mm diameter balls, a ball-to-sample weight ratio of 20:1, and a rotation speed of 300 rpm with counter-rotation occurring halfway through the time trial. These parameters were used to improve particle size reduction as small ball size, large ball-to-powder ratio, and high speeds contribute to the reduction in particle size, which also increases surface area of particles. The times tested were 6, 12, 24, and 48 h.

Carbon Powder Characterization. The characterization methods used in the temperature and ball milling time optimizations of the carbonized hydrolysis lignin are reported below with the mean value reported along with the standard deviation (SD) where applicable. Microsoft Excel 2010 was used to determine the average and standard deviation following the built in commands AVERAGE and STDEV, respectively.

Raman Spectroscopy. Raman spectra were acquired with a Renishaw Raman imaging microscope using a Renishaw NIR 780TF diode laser with a wavelength of 785 nm, and an output power of 25 mW was used for excitation with a 50× objective lens. A CCD array detector was equipped to the machine. Calibration was done using the Raman active vibration peak at 520 cm^{-1} of silicon. All spectra were obtained with the laser power set to 100% with extended scans between 500 and 2000 cm^{-1}, and they were made using 10 separate measurements of 10 s each. Deconvolution of the baselined spectra was done using PeakFit ver.4.12 software with the peak type set to Gaussian−Lorentzian area mode with a multipeak best fit with peaks present at ~1100 and ~1400 cm^{-1} along with the D and G bands.[18,19] Ratios of peak intensities were determined based on amplitude height of deconvoluted peaks.

BET Surface Area Analysis. Brunauer−Emmet−Teller (BET) surface areas of the samples were tested in a nitrogen gas sorption analysis at 77.3 K with a NOVA 4200e from Quantachrome Instruments. The calibration gas used was helium. Samples were degassed with nitrogen gas at 105 °C for 6−8 h until a stable weight was achieved before measurement. Analysis was done using the NovaWin version 10.01 software where the BET surface area was determined from a multipoint plot over the P/P_0 range of 0.05−0.35 following ASTM standard D6556-10, with the relative error calculated from the BET error table found in the NovaWin Operating Manual based on the positive C constant. The pore radius and volume were determined using the BJH pore size distribution analysis for the adsorption isotherm.

Fourier Transform Infrared Spectroscopy (FTIR). A Thermo Scientific Nicolet 6700 FTIR spectrometer in attenuated total reflectance infrared (ATR-IR) mode was used to obtain the spectra with a resolution of 4 cm^{-1} and 32 scans per sample. Powder samples of 0.1 g were pressed into disks using a Specac manual hydraulic press with a 13 mm diameter dye and a 10 ton load applied.

Particle Size Measurement. Particle sizes were measured using a laser diffractometry with a Mastersizer 2000 with a Hydro 2000SM dispersion unit (Malvern Instruments, Ltd.). The refractive indices for water and carbon were given as 1.33 and 2.42, respectively. A refractive index of 1.604 was used for lignin based on Donaldson's work.[20] The powders were dispersed in deionized water and sonicated for 5 min prior to being tested. Measurements were done in the range of 0.01 to 1000 μm using a general calculation model for spherical particles. Each sample was tested three times using a stirrer speed of 2800 rpm and an obscurance of ~5%. The data were obtained using Mastersizer 2000 software ver. 5.60.

Electrical Conductivity. Measurements of the electrical conductivity were done at room temperature using an Autolab PGSTAT302N equipped with an FRA32 M impedance analysis module from Metrohm Autolab B.V., The Netherlands. A frequency range from 400 Hz to 600 kHz was used with a 10 mV amplitude sine wave. All powder samples were oven-dried at 105 °C for 24 h, and then a mass of 0.1 g of sample was tested. Powders were placed in a hollow clear plastic cylinder with an inner diameter of 10 mm, which was then compressed between two aluminum pistons that form the electrodes. The pressure was increased from 125 kPa (due to the weight of upper piston) to 1.12 MPa by loading additional weight on top of the upper piston. This pressure range is low enough to prevent crushing of the particles while being high enough for good electrical contact between the powder and pistons. All data were acquired with Nova 1.8.17 software.

Thermal Conductivity. A Hot Disk TPS 500 Thermal Constants Analyzer from ThermTest, Inc. was used for measuring the thermal conductivity, thermal diffusivity, and volumetric heat capacity according to the transient plane source method. A 6.378 mm diameter Kapton disk type sensor was sandwiched between the carbon powders and secured by the sample holder. A total of three separate measurements were done for each powder sample. The heating power was set to 250 mW; a frequency of 60 Hz and a measurement time of 10 s were used as the testing parameters.

Scanning Electron Microscopy with Energy Dispersive X-ray Spectroscopy (SEM-EDS). Elemental analysis of the powders was done using a FEI Inspect S50 scanning electron microscope with an accelerating voltage set to 20 kV at high vacuum, with an X-Max 20 mm^2 silicon drift detector (Oxford Instruments) able to measure elements Be and above. The EDS analysis software, Aztec ver. 2.0, with the "Point & ID mode" feature was used to localize the beam onto five separate areas chosen manually within the field of view. The EDS detector measured elements above lithium and gave readings of weight percentage based on the peak heights of any element that was detected.

■ RESULTS AND DISCUSSION

Raman Spectroscopy. Raman spectroscopy of the 600, 750, and 900 °C carbonized lignin prior to ball milling was characterized to determine the microscopic structure of the carbon samples (Figure 1). It has been observed that a Raman band at ~1575 cm^{-1} is due to a single crystal of graphite, and it is known as the G peak. Another Raman band appears at ~1355 cm^{-1} in the case of polycrystalline graphite, and it is referred to as the D peak.[21] A sp^2 hybridized carbon structure is credited for both bands, with the D band being a result of the turbostratic carbon where the carbon atoms are disordered and distorted along the perimeter of the graphite sheets.[22] It is reported that the intensity ratio (I_D/I_G) of the two bands is inversely proportional to the crystallite size of the graphite (L_a).[21] In this case, as the ratio increases, an increase in disorder is also occurring as the graphene size is decreasing. Using the equation developed by Pimenta et al., the crystallite size of the graphite, L_a, in nanometers can be determined.[23]
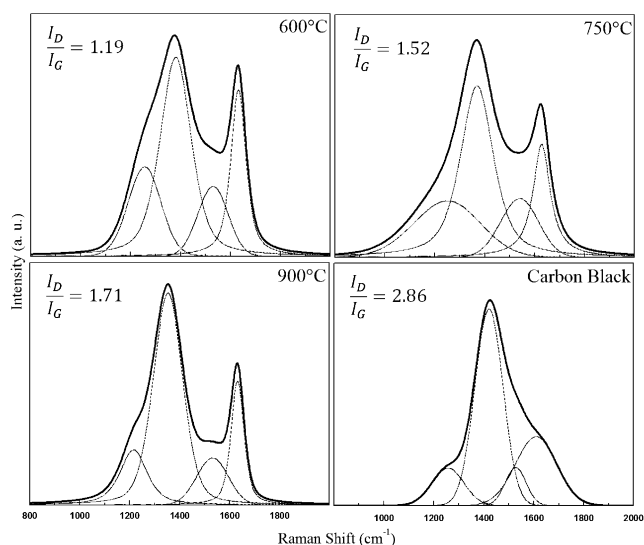
Figure 1. Deconvoluted Raman spectra of carbonized lignin at 600, 750, and 900 °C and carbon black normalized to the same height.

$$L_a = (2.4 \times 10^{-10})\lambda^4 \left(\frac{I_D}{I_G}\right)^{-1} \quad (1)$$

where λ is the wavelength of the incident laser in nanometers, and the intensity ratio of the D and G bands is unitless.

The deconvoluted spectra and the I_D/I_G intensity ratios for all carbon samples are shown in Figure 1. The D and G band ratio for all the carbonized lignin showed a gradual increase with carbonization temperature from 600 to 900 °C and an overall improvement of 44% between the 600 and 900 °C temperatures. This increase in the intensity ratio of the peaks infers that there is a larger quantity of the disordered graphite structure present at the higher temperatures. The band ratio is also able to show that the graphite regions, L_a, are decreasing in size upon increased carbonization temperatures. By using eq 1 to calculate an actual value for the crystallite size, it is found that lignin carbonized at 600 °C had a L_a value of 77 nm, while the 750 and 900 °C treatments decreased 60 and 53 nm, respectively.

The carbon black spectra has a very weak G band in comparison to the carbonized lignin samples giving rise to a larger intensity ratio of 2.86 (Figure 1), implying that the graphite regions are even smaller than those of the carbonized lignin. Again using eq 1, the value of L_a was determined to be 32 nm in size for the carbon black. The line width for the G

band of the carbon black was approximately 208 cm^{-1}, whereas the 900 °C carbonized lignin only had an approximate line width of 66 cm^{-1}, a difference of 215%, which indicates that the carbonized lignin resembles graphite more closely than the carbon black due to the narrower line width.[24]

BET Surface Area. The results from BET isotherms analysis illustrate that the bioethanol coproduct lignin prior to carbonization had a surface area of only 2 m^2 g^{-1} (Table 1), and after carbonization at 600 °C, the surface area only slightly improved. However, the higher temperature carbonization of 750 °C was able to improve the surface area to a value similar to the carbon black. A 15-fold increase in the surface area was found upon 900 °C carbonization, and an increase in pore volume was also observed. In another study where coconut shell char was analyzed, the surface area was found to increase with carbonization temperature as a result of a developing micropore structure.[25] Therefore, the substantial increase in surface area in the 900 °C carbonized lignin implies that the high temperature conditions promote the formation of pores, thus producing an activated carbon.[26]

The conductive carbon black used in this study had a surface area 955% lower than the highest temperature carbonized lignin (Table 1). Even though this conductive carbon black is within the range of surface areas associated with carbon blacks at 10 to 1000s of m^2 g^{-1}, it has been demonstrated that those powders having large surface areas have better electrical conductivity.[4] Therefore, we chose to continue the study into the effects of ball milling using the 900 °C carbonized lignin as it demonstrated the highest surface area.

After ball milling, the surface area of the carbon powder decreased (Table 1). With just 6 h of ball milling, the surface area was lowered by 23%, which can be attributed to the collapse of the pore structures during the milling process as evidenced by a reduction in pore volume. At longer ball milling times, the surface area began to increase until a maximum value of 609 m^2 g^{-1} was reached after 24 h, where it showed a pore volume exceeding the nonball milled sample. When additional ball milling was done for 48 h, a reduction in surface area was found along with a diminished pore volume. Graphitic carbon has also produced a similar trend when being ball milled, such that an increase in surface area is found initially due to fracturing of the particles from ball impacts up to a critical value, which then decreases due to particle agglomeration at longer milling times.[27] Further milling does not attain surface areas comparable to the initial maximum value.[27]

Fourier Transform Infrared Spectroscopy (FTIR). The spectra in Figure 2A shows that as the temperature was

Table 1. Surface Area, Pore Radius, and Pore Volume of Carbon Black, Lignin Treated to Various Carbonization Temperatures, and 900 °C Carbonized Lignin Treated to Different Ball Milling Times

sample		surface area (m^2 g^{-1}) ± (relative error)	pore radius (Å)	pore volume (cm^3 g^{-1})
untreated	carbon black	62^a	NA	NA
	lignin	2 ± (0.20)	16.546	0.017
carbonization temperature of lignin (°C)	600	5 ± (2.25)	16.595	0.003
	750	42 ± (1.68)	15.161	0.037
	900	654 ± (1.96)	15.168	0.13
ball milling time of 900 °C carbonized lignin (h)	6	533 ± (<1.07)	16.457	0.076
	12	563 ± (<1.13)	16.391	0.098
	24	609 ± (<1.22)	16.425	0.135
	48	580 ± (<1.16)	16.443	0.108

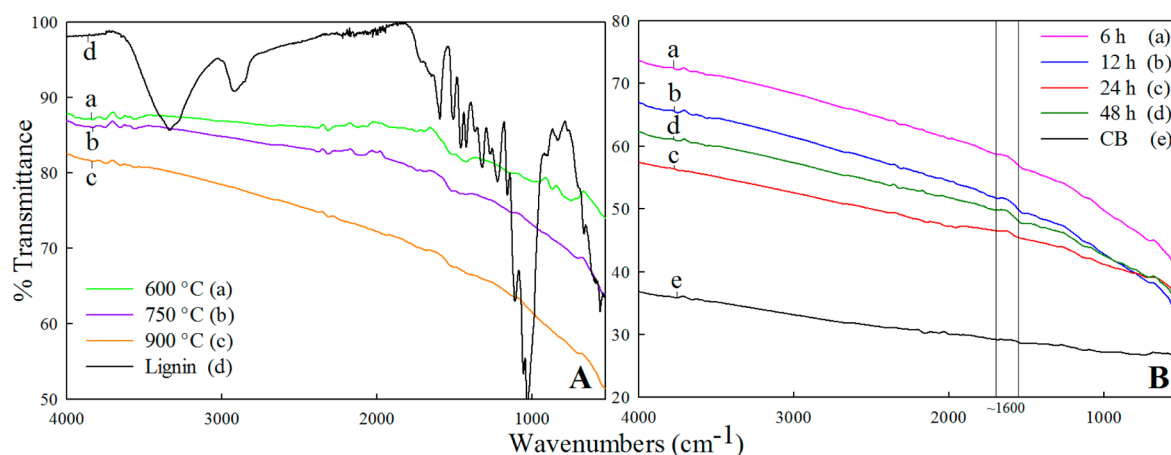^{a}Value obtained from the manufacturer.[30]

Figure 2. FTIR spectra of (A) lignin carbonized at different temperatures and (B) the 900 °C carbonized lignin sample after various ball milling times relative to carbon black.
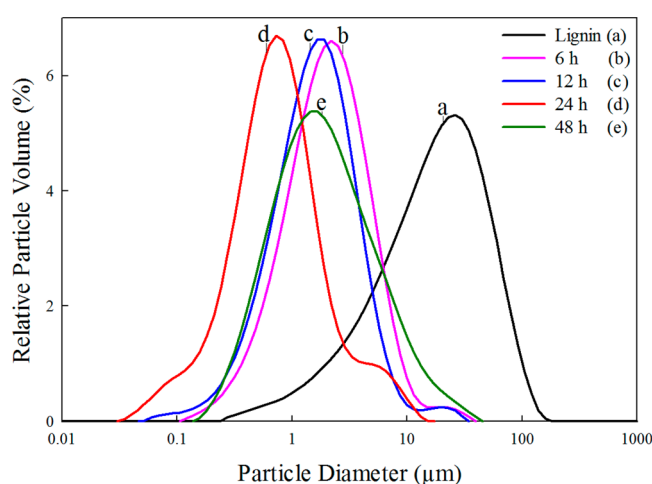

Figure 3. Distribution of particle diameters of precarbonized lignin and the 900 °C carbonized lignin after ball milling at different time intervals.
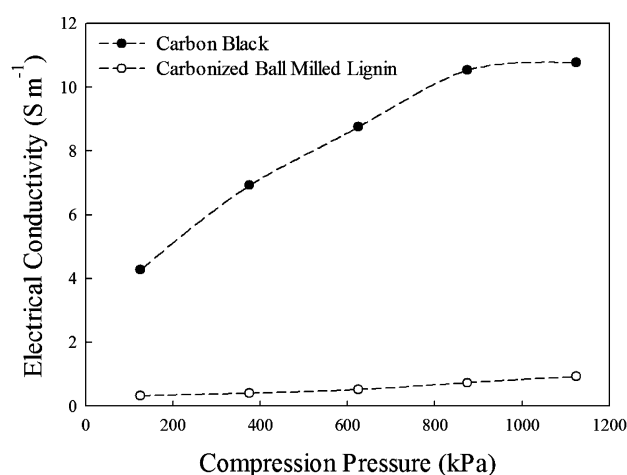

Figure 4. Electrical conductivity versus compression pressure of carbon black and 900 °C carbonized 24 h ball milled lignin.

increased the FTIR spectra smoothened to the point where the majority of the infrared peaks were removed, providing evidence that the functional groups on the lignin are removed upon carbonization. Kraft lignin has also shown this effect when

the temperature was increased from 350 to 800 °C.[28] The only prominent peak visible for the 900 °C carbonized lignin sample was found at ~1600 cm^{-1}. This absorbance is due to high conjugated C=O bonds as there remains residual oxygen species within the carbon samples that are not evident in the carbon black.[29]

Figure 2B shows that as the ball milling time was increased up to 24 h the transmittance diminished along with a reduction in the 1600 cm^{-1} peak. The decreased peak signifies minimal oxygen remaining throughout the carbon structure. The 48 h ball milled sample had a transmittance similar to the 12 h sample such that the oxygen-related peak reappears at this longer ball milling time, which can be ascribed to a lower surface area causing a reduction in IR absorbance. The 24 h ball milled sample had the greatest resemblance to carbon black as evidenced by no visible peaks and the lowest transmittance of all samples.

Particle Size. The median particle diameters for the 900 °C carbonized lignin ball milled powders were 2.185 μm, 1.742 μm, 778 nm, and 1.901 μm for the 6, 12, 24, and 48 h ball milled samples, respectively (Figure 3). These particle sizes correlate very well with the values obtained for the surface area measurements as these two properties are inversely proportional to one another. The 24 h ball milled powder had the smallest average particle size with a reduction in size of 181% occurring between 6 and 24 h. The 24 h ball milled particles contained 4% nanoparticles within the range from 1 to 100 nm, and the remainders were submicrometer to micrometer in size. The 48 h ball milled sample started to agglomerate as the size had increased back to the micrometer region.

The bioethanol coproduct lignin was determined to have a median particle diameter of 19.46 μm (Figure 3). The lignin particles are approximately 10 times larger than the carbonized ball milled powders. It should be noted that Super P Li carbon black has an aggregate size of 144 nm as calculated by the manufacturer.[30] Only the 24 h ball milled sample had a comparable size to the carbon black at the nanometer scale. Because the 24 h ball milled sample had the smallest particle size, the highest surface area, and the least oxygen species present, further characterization was only done on this powder in relation to the carbon black.

Electrical Conductivity. The conductive carbon black demonstrated an increase in conductivity from 4.3 to 10.8 S m^{-1} with increasing compression pressure up to an increase of

1260

dx.doi.org/10.1021/sc500086v | ACS Sustainable Chem. Eng. 2014, 2, 1257−1263

Table 2. Thermal Conductivity, Thermal Diffusivity, and Specific Heat of Carbon Black and 900 °C Carbonized 24 h Ball Milled Lignin (mean ± SD)

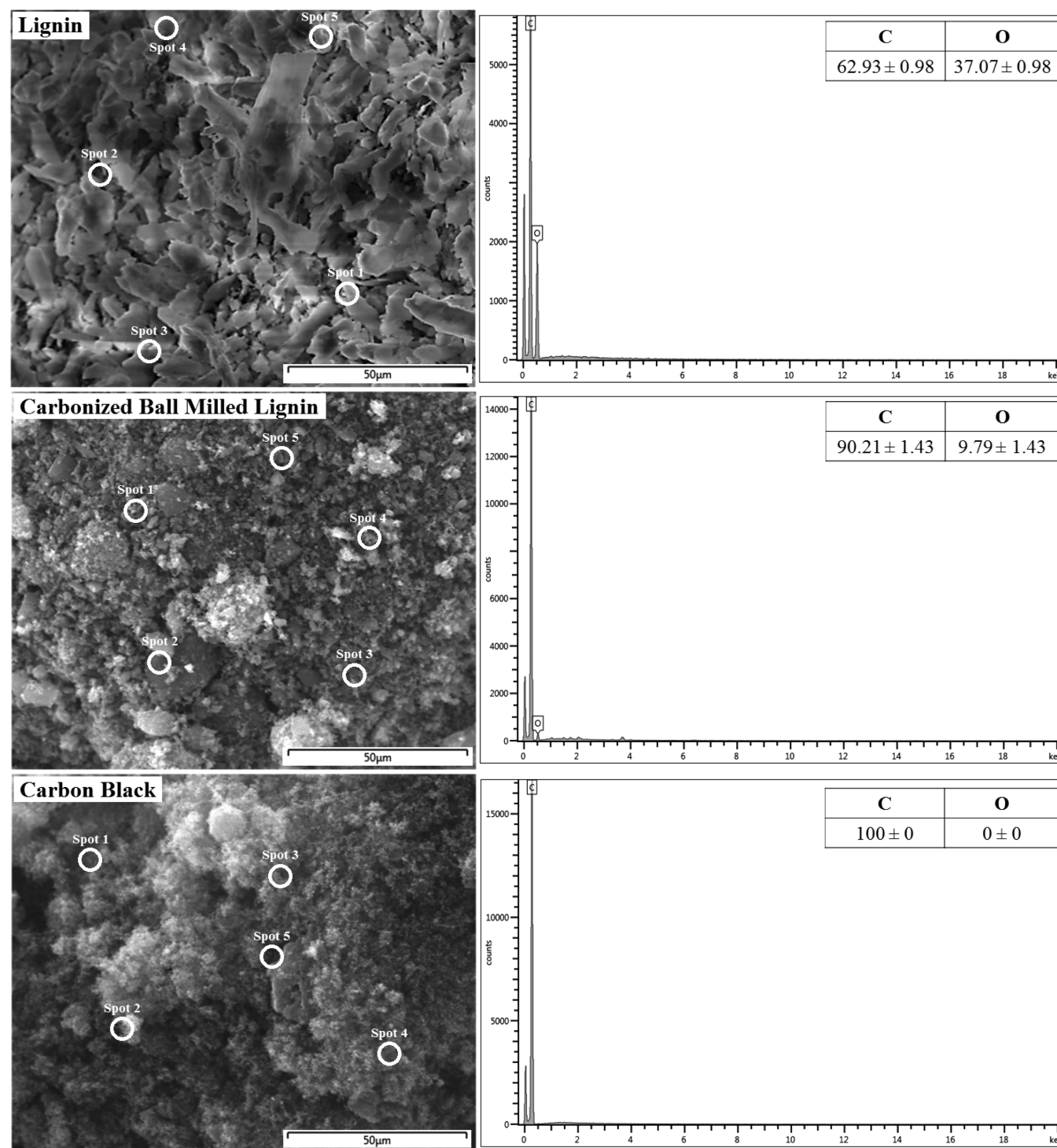| sample	thermal conductivity (W m^{-1} K^{-1})	thermal diffusivity (mm^2 s^{-1})	specific heat (MJ m^{-3} K^{-1})
carbon black	0.4924 ± 0.00035	2.949 ± 0.0040	0.1670 ± 0.00031
carbonized ball milled lignin	0.6679 ± 0.00010	1.085 ± 0.0031	0.615 ± 0.0017

Figure 5. SEM images and elemental composition of powder samples of lignin, carbonized ball milled lignin, and carbon black measured by EDS.

151% (Figure 4). The optimum carbonized ball milled lignin powder only increased in conductivity from 0.3 to 0.9 S m^{-1}. The carbonized lignin did not show an overall improvement in its conductivity, whereas the carbon black more than doubled over the pressure range. A difference of 9.5 S m^{-1} is found between the conductivities of the carbon black and optimized powder at the highest pressure tested. The difference in the electrical conductivity of the carbonized lignin and the carbon

black may be attributed to the reduced oxygen species in carbon black based on FTIR spectra (Figure 2), whereas the ball milled carbonized lignin contains residual oxygen. Surface elements other than carbon are known to decrease the overall conductivity of the material.[31]

Electrical conductivity is enhanced when a reduction in the powder volume occurs at the higher pressure loadings.[32] This helps to explain why the carbon black had a more pronounced improvement in its conductivity because its volume decreased by 43% at 1.12 MPa, whereas the carbonized ball milled lignin only showed a reduction in volume of 24% (data not shown). The carbon black in the present study showed a similar response to carbon black powder under analogous measurement conditions.[33]

Thermal Conductivity. Carbon structures are considered to be thermally stable, and carbon black has been shown to improve thermal conductance.[34] Therefore, the optimized 900 °C carbonized 24 h ball milled lignin sample was analyzed in comparison to the carbon black for their thermal properties. The data in Table 2 show that the carbonized ball milled lignin had a 36% higher thermal conductivity than that of the carbon black powder. This difference between the two carbon powders can be attributed to the size difference of the particles, as the larger the particle size is the greater the conductivity of the carbon powder is.[35] This occurs because thermal conductance relies on the thermal energy transfer within the particles, locations of direct contact of adjacent particles, and radiant heat transferred to neighboring particles. A bigger particle has a larger contact area than a fine particle, and it contains a greater number of pores and cavities that contribute to the radiant heat, which will reduce the thermal resistance and in turn improve the thermal conductance. The thermal conductance for both carbons fall within the range of $0.01-2$ W m^{-1} K^{-1} for amorphous carbon made up of a combination of sp^2 and sp^3 bonding.[36]

Thermal diffusivity of carbon black was approximately three times greater than that found for the carbonized ball milled lignin sample (Table 2). The carbon black more readily disperses the conducted heat because of its aciniform structure, which is made of fused spherical primary particles, such that the fused locations act as connective pathways in which heat can be distributed swiftly from one primary particle to the next. The volumetric heat capacity exhibited a difference of 268% between the two powders (Table 2) such that the carbonized ball milled lignin showed a relatively high specific heat compared with that of the carbon black. The differences in the heat capacities may be a result of the lower bulk density of carbon black compared with that of the carbonized ball milled lignin.

Scanning Electron Microscopy with Energy Dispersive X-ray Spectroscopy (SEM-EDS). The elemental composition of carbon and oxygen in various powders was determined using energy dispersive spectroscopy (EDS) (Figure 5), although hydrogen cannot be detected using this analysis method. The untreated lignin SEM image is slightly distorted as a result of charging; however, this did not affect the elemental analysis, which only showed elemental traces for carbon and oxygen when performing the Point & ID analysis at the five locations shown in Figure 5. Kraft lignin also is mainly composed of these two elements.[13] For both the untreated lignin and the carbonized ball milled lignin, the primary constituent was carbon, and smaller traces of oxygen remained after carbonization, indicating that not all oxygen functional groups would be removed under this carbonization process. In the case of carbon black, only elemental carbon was detected with no oxygen present. Other carbon blacks have also shown minimal to no oxygen existing within the powders.[4,31] The difference in oxygen content between the carbonized ball milled lignin and the carbon black explains the reduced conductivity, as surface elements other than carbon hinder electrical conductance through the powder.

CONCLUSION

A carbonaceous powder was successfully produced using bioethanol coproduct lignin and characterized against carbon black to optimize carbonization temperature and ball milling time. Raman analysis demonstrated a higher graphitic nature for the carbonized lignin than the carbon black under investigation. The BET surface area was larger in the case of carbonized lignin as a result of the porosity of the powder. Higher temperature carbonization and ball milling times up to 24 h reduced unwanted oxygen species on the carbon surface as seen by FTIR. Carbonized lignin nanoparticles were formed after 24 h of ball milling that fall within the same order of magnitude in size as the carbon black aggregates. The conductivity measurements showed inferior electrical conductivity while having superior thermal conductance. SEM-EDS displayed the carbon purity of the carbonized lignin to be above 90% close to the highly pure carbon black powder. With the only drawback of this carbonized ball milled lignin being the electrical conductivity, the possibility of using the powder as an alternative to carbon black is feasible when applied to nonelectrical applications. These applications include nonconductive black ink, toner, paint, thermal paste, and thermally conductive filler.

AUTHOR INFORMATION

Corresponding Author
*E-mail: mmisra@uoguelph.ca. Tel.:+1-519-824-4120, ext. 58935, 56766. Fax: +1-519-836-0227.

Notes
The authors declare no competing financial interest.

ACKNOWLEDGMENTS

REFERENCES

(1) Shenderova, O.; Zhirnov, V.; Brenner, D. Carbon nanostructures. *Crit. Rev. Solid State Mater. Sci.* **2002**, *27*, 227−356.

(2) Dresselhaus, M. S.; Dresselhaus, G.; Eklund, P. C. *Science of Fullerenes and Carbon Nanotubes: Their Properties and Applications*; Academic Press: San Diego, CA, 1996.

(3) Rahman, A.; Ali, I.; Al Zahrani, S. M.; Eleithy, R. H. A review of the applications of nanocarbon polymer composites. *Nano* **2011**, *6*, 185−203.

(4) Pantea, D.; Darmstadt, H.; Kaliaguine, S.; Roy, C. Electrical conductivity of conductive carbon blacks: Influence of surface chemistry and topology. *Appl. Surf. Sci.* **2003**, *217*, 181−193.

(5) Zhang, W.; Dehghani-Sanij, A. A.; Blackburn, R. S. Carbon based conductive polymer composites. *J. Mater. Sci.* **2007**, *42*, 3408−3418.

(6) Glatz-Reichenbach, J. Conducting polymer composites. *J. Electroceram.* **1999**, *3*, 329−346.

(7) Huang, J. Carbon black filled conducting polymers and polymer blends. *Adv. Polym. Technol.* **2002**, *21*, 299−313.

(8) Lahaye, J.; Ehrburger-Dolle, F. Mechanisms of carbon black formation. Correlation with the morphology of aggregates. *Carbon* **1994**, *32*, 1319−1324.

(9) Carrott, P.; Ribeiro Carrott, M. Lignin−from natural adsorbent to activated carbon: A review. *Bioresour. Technol.* **2007**, *98*, 2301−2312.

(10) Kadla, J.; Kubo, S.; Venditti, R.; Gilbert, R.; Compere, A.; Griffith, W. Lignin-based carbon fibers for composite fiber applications. *Carbon* **2002**, *40*, 2913−2920.

(11) Babeł, K.; Jurewicz, K. KOH activated lignin based nano-structured carbon exhibiting high hydrogen electrosorption. *Carbon* **2008**, *46*, 1948−1956.

(12) Lora, J. H.; Glasser, W. G. Recent industrial applications of lignin: a sustainable alternative to nonrenewable materials. *J. Polym. Environ.* **2002**, *10*, 39−48.

(13) Kumar, S.; Mohanty, A.; Erickson, L.; Misra, M. Lignin and its applications with polymers. *J. Biobased Mater. Bioenergy* **2009**, *3*, 1−24.

(14) Fu, K.; Yue, Q.; Gao, B.; Sun, Y.; Zhu, L. Preparation, characterization and application of lignin-based activated carbon from black liquor lignin by steam activation. *Chem. Eng. J.* **2013**, *228*, 1074−1082.

(15) Gonugunta, P.; Vivekanandhan, S.; Mohanty, A. K.; Misra, M. A study on synthesis and characterization of biobased carbon nano-particles from lignin. *World* **2012**, *2*, 148−153.

(16) Hayashi, J.; Kazehaya, A.; Muroyama, K.; Watkinson, A. P. Preparation of activated carbon from lignin by chemical activation. *Carbon* **2000**, *38*, 1873−1878.

(17) Poursorkhabi, V.; Misra, M.; Mohanty, A. K. Extraction of lignin from a coproduct of the cellulosic ethanol industry and its thermal characterization. *BioResources* **2013**, *8*, 5083−5101.

(18) Ferrari, A.; Robertson, J. Interpretation of Raman spectra of disordered and amorphous carbon. *Phys. Rev. B* **2000**, *61*, 14095.

(19) Hauptman, N.; Vesel, A.; Ivanovski, V.; Gunde, M. K. Electrical conductivity of carbon black pigments. *Dyes Pigm.* **2012**, *95*, 1−7.

(20) Donaldson, L. A. Critical assessment of interference microscopy as a technique for measuring lignin distribution in cell walls. *N. Z. J. For. Sci.* **1985**, *15*, 349−360.

(21) Tuinstra, F.; Koenig, J. L. Raman spectrum of graphite. *J. Chem. Phys.* **1970**, *53*, 1126.

(22) Paris, O.; Zollfrank, C.; Zickler, G. A. Decomposition and carbonisation of wood biopolymers—A microstructural study of softwood pyrolysis. *Carbon* **2005**, *43*, 53−66.

(23) Pimenta, M.; Dresselhaus, G.; Dresselhaus, M. S.; Cancado, L.; Jorio, A.; Saito, R. Studying disorder in graphite-based systems by Raman spectroscopy. *Phys. Chem. Chem. Phys.* **2007**, *9*, 1276−1290.

(24) Tuinstra, F.; Koenig, J. Characterization of graphite fiber surfaces with Raman spectroscopy. *J. Composite Mater.* **1970**, *4*, 492−499.

(25) Li, W.; Yang, K.; Peng, J.; Zhang, L.; Guo, S.; Xia, H. Effects of carbonization temperatures on characteristics of porosity in coconut shell chars and activated carbons derived from carbonized coconut shell chars. *Ind. Crops Prod.* **2008**, *28*, 190−198.

(26) Cao, Q.; Xie, K.; Lv, Y.; Bao, W. Process effects on activated carbon with large specific surface area from corn cob. *Bioresour. Technol.* **2006**, *97*, 110−115.

(27) Chen, Y.; Fitz Gerald, J.; Chadderton, L. T.; Chaffron, L. Nanoporous carbon produced by ball milling. *Appl. Phys. Lett.* **1999**, *74*, 2782−2784.

(28) Rodríguez-Mirasol, J.; Cordero, T.; Rodríguez, J. Preparation and characterization of activated carbons from eucalyptus kraft lignin. *Carbon* **1993**, *31*, 87−95.

(29) O'Reilly, J.; Mosher, R. Functional groups in carbon black by FTIR spectroscopy. *Carbon* **1983**, *21*, 47−51.

(30) Spahr, M. E.; Goers, D.; Leone, A.; Stallone, S.; Grivei, E. Development of carbon conductive additives for advanced lithium ion batteries. *J. Power Sources* **2011**, *196*, 3404−3413.

(31) Pantea, D.; Darmstadt, H.; Kaliaguine, S.; Sümmchen, L.; Roy, C. Electrical conductivity of thermal carbon blacks: Influence of surface chemistry. *Carbon* **2001**, *39*, 1147−1158.

(32) Sanchez-Gonzalez, J.; Macias-Garcia, A.; Alexandre-Franco, M.; Gómez-Serrano, V. Electrical conductivity of carbon blacks under compression. *Carbon* **2005**, *43*, 741−747.

(33) Celzard, A.; Marêché, J.; Payot, F.; Furdin, G. Electrical conductivity of carbonaceous powders. *Carbon* **2002**, *40*, 2801−2815.

(34) Leong, C.; Chung, D. Carbon black dispersions as thermal pastes that surpass solder in providing high thermal contact conductance. *Carbon* **2003**, *41*, 2459−2469.

(35) Khizhnyak, P.; Chechetkin, A.; Glybin, A. Thermal conductivity of carbon black. *J. Eng. Phys.* **1979**, *37*, 1073−1075.

(36) Balandin, A. A. Thermal properties of graphene and nanostructured carbon materials. *Nat, Mater.* **2011**, *10*, 569−581.